Taylor-Couette Unit with a Lobed Inner Cylinder Cross Section

Miroslav Soos, Hua Wu, and Massimo Morbidelli
Institute for Chemical and Bioengineering, Dept. of Chemistry and Applied Biosciences, ETH Zurich, 8093 Zurich, Switzerland

DOI 10.1002/aic.11153
Published online March 20, 2007 in Wiley InterScience (www.interscience.wiley.com).

A new mixing unit, based on a modification of the classical Taylor-Couette (TC) unit is proposed, where a lobed profile of the inner cylinder cross section is used. The shear rate distribution of the lobed Taylor-Couette (LTC) unit have been computed through computational fluid dynamic simulations and compared with those of the TC unit and a standard stirred tank (ST). It is found that since the flow pattern of the LTC units becomes temporal-periodic at each point with respect to the nonrotational outer cylinder, it reduces the formation of the low velocity gradient (low shear rate) region, typically generated in the vortex core of the TC units. The obtained distributions of the shear rate are substantially narrower than those of the TC and the ST units. Variation of the ratio between the maximum and the minimum gap widths can lead to significant changes in the shear rate distribution, and there exists an optimal range of such ratio, where the shear rate distribution is not only very narrow but also insensitive to the variation of the gap widths. © 2007 American Institute of Chemical Engineers *AIChE J,* 53: 1109–1120, 2007

Keywords: Taylor-Couette, mixing unit, reactor, shear rate, computational fluid dynamic, turbulent flow

Introduction

Taylor Couette (TC) flow as a model secondary flow system for fundamental studies in fluid mechanics has been widely investigated since the Taylor pioneering work in 1923. Its specific flow features such as rather narrow shear rate distribution, absence of high shear rate regions with respect to conventional stirred-tank reactors, flow pattern covering limits from almost plug flow to ideally stirred tank (ST) reactor, etc., have potential applications in practice. However, only in the last 20-years these features have been considered for realizing units of interest for chemical engineering applications. For example, the TC reactor was successfully used for continuous emulsion polymerization to reduce shear-induced coagulation as well as to increase the monomer conversion.[1,2] The TC unit was also used as a filtration unit to improve the mass transfer for filtering mixtures containing fragile components.[3–6] Because of the absence of the high shear regions with respect to conventional stirred-tank reactors, it was successfully applied as a biochemical reactor for various systems including yeasts,[7,8] mammalian cells,[9] and blood cells[10–13] or as a precipitator for reducing breakage of crystals.[14] Since the Taylor vortexes force the fluid to periodically experience the surfaces of the inner and outer cylinders, the TC unit can be used as a support for catalyst or light source for photocatalytic reactions.[15–20] Moreover, as shown by Baier et al.,[21] highly active interfacial surface between two counter-currently rotating vortexes can be used to improve the liquid-liquid extraction efficiency.

Some limitations in the mixing process in the TC unit have been evidenced, e.g. when the TC unit operates in the laminar flow regime, mixing in the core of the vortexes occurs through pure molecular diffusion, thus leading to significant deficiencies in terms of intra-vortex mixing.[22]

Correspondence concerning this article should be addressed to M. Morbidelli at massimo.morbidelli@chem.ethz.ch.

Moreover, when particles or bubbles are present as a secondary phase in the TC reactor, Resende et al.[23] have experimentally observed that due to the inertial forces the dispersed phase is concentrated more in the core of the vortexes, where velocities as well as shear rates are low. Drozdov[24] used particles of different relative densities to the disperse phase in the TC unit with undulated surfaces of both cylinders along the axial direction and observed through numerical simulations that the high probability region of particles is strongly correlated with the regions of low velocity (or shear rate). As a result, the mean residence time of the dispersed phase in the reactor is longer than that of the continuous phase when the TC units operate in the continuous mode. Such segregation effect could be undesired for particulate systems.

A way to overcome this segregation, while keeping the main advantage of the TC flow, is to eliminate or reduce the low velocity (or low shear rate) regions in the TC flow so as to further narrow the shear rate distribution in the TC unit, thus improving mixing within and between the vortexes. One of the possible solutions is to locate eccentrically the inner cylinder of the TC unit[25–29] to break the rotational symmetry of the flow, thus improving the mixing or shear rate distribution. Lopez and Marques[30] proposed to rotate the inner cylinder at a constant angular velocity and simultaneously to rotate or move the outer cylinder at a velocity properly modulated in time. From the practical point of view rotating both inner and outer cylinders simultaneously is rather difficult. Snyder[31] and Mullin and Lorenzen[32] observed that using a square cross section of the inner cylinder or outer cylinder can affect significantly the flow pattern and consequently the mixing intensity in the vortexes with respect to the classical TC unit.

In this work, we propose to reduce the low velocity (or shear rate) regions in the TC unit, thus improving the shear rate distribution or the intra-vortex mixing, through a proper design of the cross-section of the inner cylinder.[33] In particular, the circular cross-section of the inner cylinder is substituted by a lobed one. This leads to a unit, referred to in the following as the Lobed Taylor-Couette (LTC) unit, where the gap between the inner and outer cylinder is not constant. The specific profile, i.e. the nonconstant gap, is designed so as to deform or reduce the Taylor vortexes and therefore to improve the flow intensity and mixing in the core of the vortexes. As a consequence, the distribution of the shear rate within the gap becomes substantially narrower than that of the classical TC units. The design of the LTC unit is performed in this work through numerical simulations using the commercial computational fluid dynamic (CFD) package, Fluent v6.2. The distributions of shear rate and power input of the LTC units are computed and compared with those of the classical TC as well as the typical ST equipped with the Rushton turbine. The experimental validation is limited to the values of the torque as a function of the Reynolds number.

The CFD Simulation Procedure

Geometry of the LTC unit

To investigate the possibility of improving the distribution of the shear rate γ in the unit by properly designing the profile of the inner cylinder cross section, we consider three different shapes with ellipse- or triangle- or square-type of profile. In Figure 1 is shown the cross-section of the LTC unit with a triangle-type of profile, where R_o is the radius of the outer cylinder, and the parameters, d_{min} and d_{max}, are the minimum and maximum widths of the gap between the inner and outer cylinders. The cross section profile of the inner cylinder is constructed by connecting three circles with the same radius R_c ($=R_o - 2d_{max} + d_{min}$), positioned 120° with respect to each other, and shifted eccentrically from the axis of the outer cylinder by a distance e ($=2^*$ ($R_o - d_{max} - R_c$)). The connection is made along their mutual tangential lines. In this study, the values for R_o and d_{min} are fixed to be 70 and 8 mm, respectively, while the maximum gap width, d_{max} varies from 8 to 22 mm. Obviously, at $d_{max} = 8$ mm, the LTC unit reduces to the classical TC unit with the ratio of the inner to outer cylinder radius, η, equal to 0.886. The length of the LTC reactor, L, is equal to 320 mm. This leads to the aspect ratio Γ of the minimum gap width d_{min} to the reactor length L equal to 40. The square-type cross section geometry of the inner cylinder is constructed by connecting four circles with the same radius R_c ($=[a - b\cos(\pi/4)]/[1 - \cos(\pi/4)]$), where $a = (R_o - d_{max})$, and $b = (R_o - d_{min})$. The four circles are positioned 90° with respect to each other and shifted eccentrically from the axis of the outer cylinder by a distance e ($=(R_o - d_{min} - R_c)$. As in case of the triangle cross section, the connection is made along their mutual tangential lines, the values for R_o and d_{min} are 70 and 8 mm, respectively, and the maximum gap width, d_{max}, varies from 8 to 22 mm.

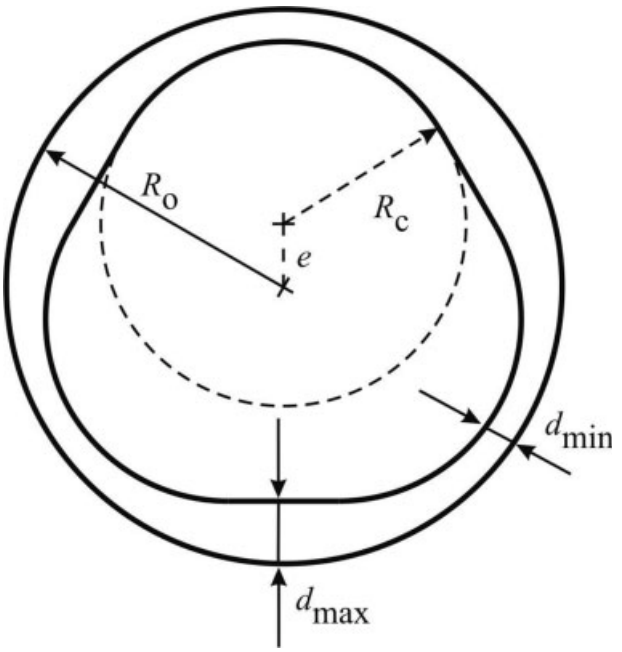

Figure 1. Schematic of the cross section of the inner cylinder perpendicular to the rotation axis of a LTC unit in the case of a triangle-type profile.

Numerical simulations

Currently, there is no convenient technique to measure directly the distribution of the energy dissipation rate ε in

mechanically stirred units, which is then used to evaluate the distribution of the shear rate γ, though $\gamma = \sqrt{\varepsilon/\nu}$ under turbulent conditions.[34] However, it is possible, using laser Doppler velocimetry (LDV)[35] and particle image velocimetry (PIV),[9,36–40] to measure the velocity profiles (instantaneous as well as time averaged) and flow patterns. From the components of the mean velocity and the velocity fluctuations it is possible to estimate the ε distribution, and consequently the γ distribution. However, the LDV and PIV techniques are difficult to apply to the present LTC unit, because the deformed inner cylinder leads to a flow pattern varying periodically with time with respect to a fixed location inside the gap. On the other hand, it has been confirmed that simulations of the single-phase flow using commercial softwares for CFD, such as Fluent, CFX, and StarCD, can correctly reproduce the average velocity profiles and flow patterns measured by LDV and PIV techniques.[9,40–43] Therefore, in the following we rely on single-phase CFD simulations, using the commercial software, Fluent (version 6.2), to compute the shear rate distribution as well as the other fluid dynamic properties in the various units considered in this work.

All simulations are carried out in 3D, where only one half of the unit height is simulated because of its geometrical symmetry. The initial computation grid is set as follows: 20 nodes in the radial direction, 160 nodes in axial direction, and 160–420 nodes in the circumferential direction depending on the d_{max} value. In addition, points in the gap were distributed asymmetrically to properly resolve the local large gradients near the inner and outer walls. Thus, the total number of the initial computational cells (for 1/2 of the reactor height) varies from 512,000 to 1,344,000. During the simulations several adaptations were applied to improve the quality of the mesh in the regions with larger velocity gradients so as to obtain the mesh independent solution. In the viscous sublayer near the wall the standard wall function (SWF) was used in all simulations, where the size of the first volume element (characterized by y^+ $(=\rho u_\tau y/\mu)$) was kept approximately constant (=30) for all investigated geometries.

The turbulent flow can be simulated within Fluent using different models to close the Reynolds averaged momentum balance equations. It was found by Marchisio et al.,[44] that the Reynolds Stress Model leads to the best agreement with the experimental data in the case of the TC units. Therefore, in all the following simulations this model has been used in combination with the SWF. It is worth noting that due to the narrow gap in the TC and LTC units, where a relatively large portion of the energy is dissipated near the wall, one would expect the nonequilibrium wall function to better handle the fine structure of the flow close to the wall. However, our simulation results indicate that, at least for the conditions considered in this work, the two approximations do not lead to significant differences. The rotation of the inner wall is implemented by a rotating reference frame where the liquid rotates with the same velocity as the inner cylinder, and the outer cylinder is treated as static.[18]

It is worth mentioning that when we compute directly the steady-state conditions of the TC and LTC units, some difficulties have been encountered, particularly for small differences between d_{min} and d_{max}. As mentioned by Haut et al.,[9] the solution of the steady-state is very sensitive to the first trial solution. One example of the temporal solution for a TC unit starting from the uniform velocity profile using steady-state simulation after few iteration steps is shown in Figure 2a, where a radial component of the velocity on the unwrapped circumferential surface in the middle of the gap of the TC unit is plotted. Continuation of such nonrealistic partially converged solution requires substantially long computational time to reach correct solution. In fact, Haut et al.[9] solve this problem using experimentally measured velocity profile from the PIV technique as a first trial solution. Since we do not have experimental data for our geometry and further the deformation of the inner cylinder introduces another type of instability to the flow field, in all our simulations we use the time-dependent mode. This avoids the abnormal flow patterns as shown in Figure 2a. Note that the results in Figure 2b,c correspond to the simulations of one half of the total height of the TC, where the top part of the velocity profile is attached to the static wall and the bottom part to the symmetry boundary. Moreover, for a geometry of the TC similar to the one used in this study, Koschmieder[45] showed experimentally the existence of multiple steady-state solutions in terms of number of vortexes (or wavelength λ). In fact with varying first trial solutions, we have also observed multiple steady-state solutions with respect to the number of the vortexes where the wavelength λ varies in the range from 2.5 to 3.5, in agreement with the results obtained by Koschmieder.[45]

Results and Discussion

The classical Taylor-Couette unit

Before discussing the simulation results of the LTC unit, let us first consider the classical TC unit. This step is necessary since some experimental data of the flow field in the TC units are available in the literature, and in this case we can validate the CFD simulation procedure described earlier. For this, the average axial velocity profile in the gap of the TC unit measured by Haut et al.[9] using the PIV technique has been simulated. The inner and outer cylinders have radii equal to 40 and 48.5 mm, respectively. The experimental results at the rotation speed of the inner cylinder, equal to 2.15 rad/s, are shown in Figure 3 by the symbols (▲), where z is the axial coordinate, and U_{ax} is the mean axial velocity on the circumferential surface with distance of 2.125 mm from the surface of the inner cylinder. The solid curve represents the corresponding mean axial velocity profile computed through 3D simulations. It is seen that the agreement between experiments and numerical simulations is very satisfactory.

As a second check of the adopted CFD simulation procedure, we have computed the torque on the inner cylinder of the TC unit as a function of the rotation speed and compared the results with the experimental measurements. The used TC unit has internal and external radii equal to 62 and 70 mm, respectively, with height equal to 320 mm. The inner cylinder is made of polished stainless steel, while the outer cylinder is of precise glass (Schott, Duran®). The torque on the inner cylinder is measured using a torque meter (MCRT28001T-25-0-NA, Himmelstein & Co) mounted between the motor and the rotating shaft. The range of the rotation speed of the inner cylinder is selected in such a way

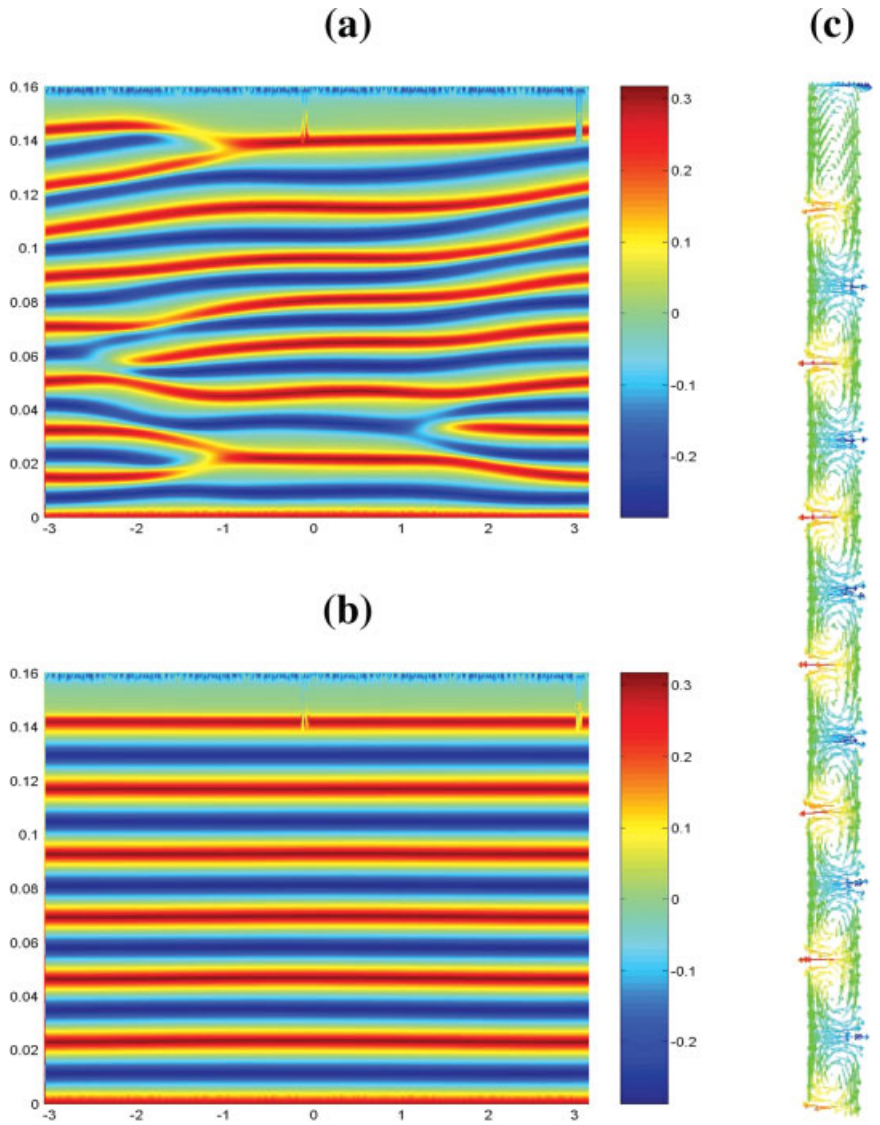

Figure 2. Steady-state radial velocity pattern on the unwrapped circumferential surface in the middle of the gap for a TC unit: (a) direct steady-state simulation; (b) simulation of the entire transient evolution; (c) radial velocity pattern in the gap of the TC corresponding to (b).

[Color figure can be viewed in the online issue, which is available at www.interscience.wiley.com.]

that the flow in the gap is always turbulent. At each rotation speed, the torque values are measured for the TC unit filled with deionized water and empty, and the difference between the two values gives the net torque on the inner cylinder. Figure 4 shows a comparison between CFD simulations and experimental data, where G and Re are the dimensionless torque and the Reynolds number defined as

$$G = \frac{\tau}{\rho v^2 L}; \quad Re = \frac{R_i \Omega d}{v} \tag{1}$$

where τ is the torque on the surface of the inner cylinder, ρ and v are the density and the kinematic viscosity of the fluid, respectively, Ω and R_i are the angular velocity and the radius of the inner cylinder, and d is the gap width. It is seen that the agreement between simulations and experiments is rather satisfactory in the entire range of Re values. Lathrop et al.[46] developed the following correlation between G and Re based on the experimental data of Wendt[47]:

$$G = \begin{cases} 1.45 \dfrac{\eta^{3/2}}{(1-\eta)^{7/4}} Re^{1.5} & \text{for} \quad 4 \times 10^2 < Re < 10^4 \\ 0.23 \dfrac{\eta^{3/2}}{(1-\eta)^{7/4}} Re^{1.7} & \text{for} \quad 10^4 < Re < 10^5 \end{cases} \tag{2}$$

where η ($=R_i/R_o$) is the ratio between the radius of the inner and outer cylinder. The solid curve in Figure 4 corresponds to the results of Eq. 2 for the TC unit considered in this work. Again, they are in good agreement with our experimental data and CFD simulations.

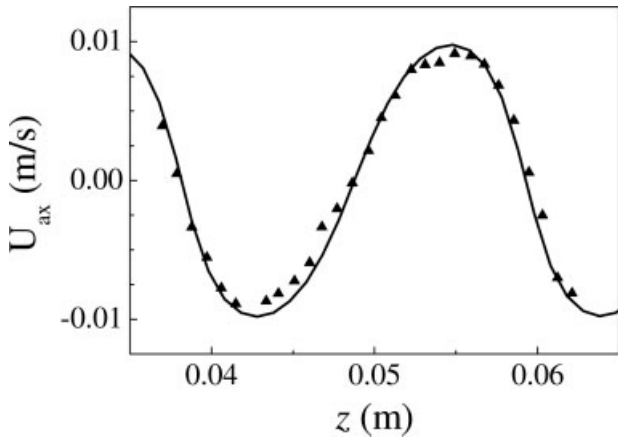

Figure 3. Time-average axial velocity profile on the circumferential surface at a distance of 2.125 mm from the surface of the inner cylinder, at the angular velocity Ω = 2.15 rad/s. (▲) experimental data by Haut et al.,[9] (solid curve) CFD simulation. R_o = 4.85 mm; d = 8.5 mm.

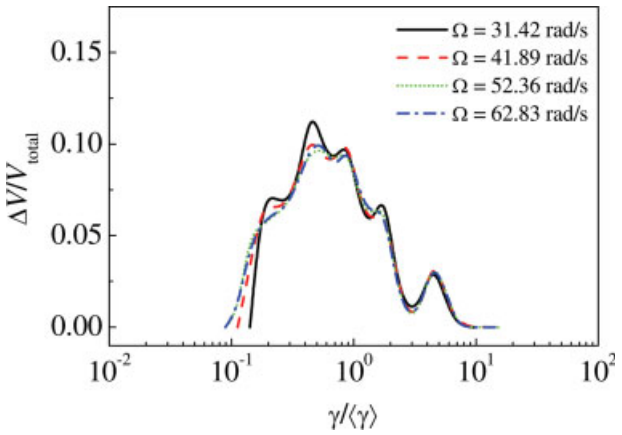

Figure 5. Distributions of the normalized shear rate, $\gamma/\langle\gamma\rangle$, for the TC unit at various rotation speeds of the inner cylinder, Ω. R_o = 70 mm; d = 8 mm.

[Color figure can be viewed in the online issue, which is available at www.interscience.wiley.com.]

In Figure 5 are presented the distributions of the shear rate γ normalized by the volume-averaged shear rate $\langle\gamma\rangle$, computed for the TC unit with $R_o = 70$ mm and $d = 8$ mm, corresponding to the four angular velocities of the inner cylinder used in Figure 4. It is seen that in all the four cases the shape of the shear rate distribution is rather similar and covers approximately two orders of magnitude. There is only a slight increase in the broadness of the distribution, as the angular velocity increases. On the other hand, as shown by various authors,[9,23,46] increasing the rotation speed of the inner cylinder improves the mass transport within and between the vortexes.

A comparison between the normalized shear rate distributions of the TC unit considered earlier and a standard ST (equipped with a Rushton turbine operated under turbulent conditions as defined by Wu and Patterson[35]] is presented in Figure 6. For the ST, similar to the TC geometry, several refinements of the computational grid have also been performed in order to obtain mesh independent solution. We use this ST geometry because the experimental data reported by Wu and Patterson[35] can be used as a further validation of the adopted CFD simulation procedure, as discussed in the Appendix. As expected, the normalized shear rate distribution of the ST shown in Figure 6 is much broader than that of the TC unit, and in fact covers at least three orders of magnitude. This is due to the presence of two regions in the ST, one close to the impeller and one at the top of the vessel far from the impeller, exhibiting very large and very small shear rates, respectively. It is the absence of this region of high shear rates that makes TC unit desirable for stirring mixtures containing shear sensitive components.[2,9,11,14]

On the other hand, as mentioned in the Introduction, when a dispersed phase is present, the TC flow may lead to concentrating particles,[23] droplets[41,48] or bubbles (observation

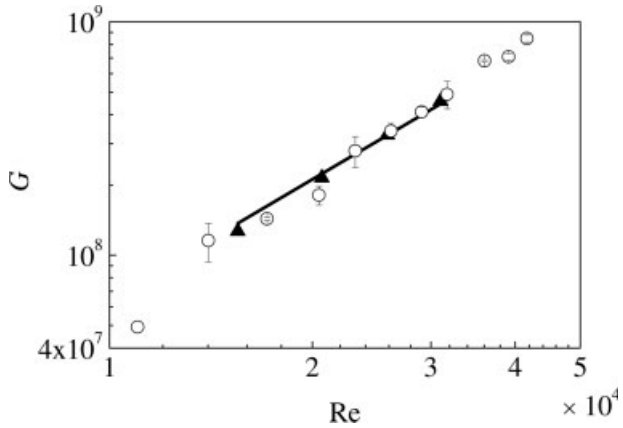

Figure 4. Values of the dimensionless torque G on the surface of the inner cylinder as a function of the Reynolds number, Re, for a TC unit. (▲) CFD simulations; (○) experimental data; (—) Eq. 2. R_o = 70 mm; d = 8 mm.

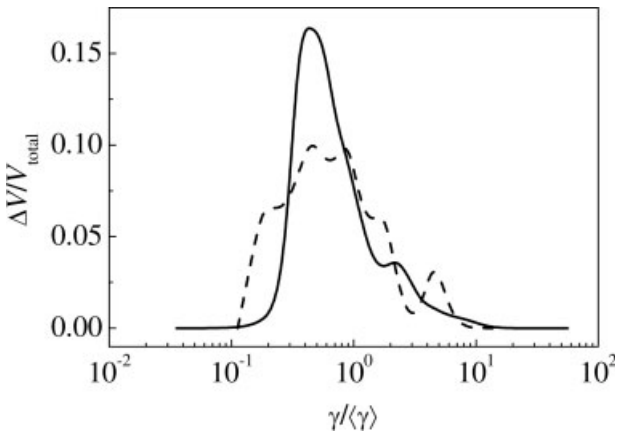

Figure 6. Distributions of the normalized shear rate, $\gamma/\langle\gamma\rangle$, for a TC unit (– – –) and a stirred tank with Rushton turbine (—). R_o = 70 mm; d = 8 mm, $\langle\gamma\rangle$ = 685 s^{-1}.

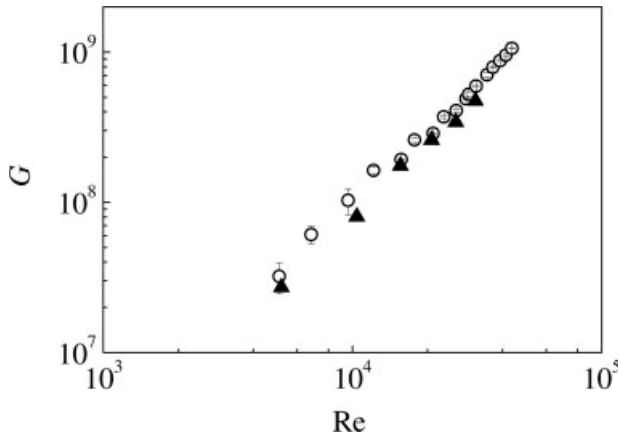

Figure 7. Values of the dimensionless torque *G* on the surface of the inner cylinder as a function of the Reynolds number, *Re*, for a lobed TC with triangular shape of the inner cylinder cross section. (▲) CFD simulations, (○) experimental data.

from our laboratory) in the region with smaller velocity gradient, i.e., in the core of the vortexes. This arises because in the region of small velocity fluctuations, the particles tend to follow closely the trajectories of the fluid. Such a segregation behavior can lead to inhomogeneity in the system, which is undesired in most industrial applications.

In addition, although the normalized shear rate distribution of the TC unit is much narrower than that of the ST, it still covers at least two orders of magnitude. This leads to the introduction of the LTC unit to reduce the above drawbacks.

The lobed Taylor-Couette unit

Let us first consider the LTC unit with a triangular shape of the inner cylinder cross section as drawn in Figure 1. To validate the results obtained from the CFD simulation, we have performed series of experiments to measure the torque on the surface of the inner cylinder, using the same procedure described in the context of Figure 4. The used LTC unit has dimensions: $R_o = 70$ mm, $d_{min} = 8$ mm, $d_{max} = 12$ mm, and height equal to 320 mm. Comparison of the torque values obtained experimentally with those from the CFD simulations is presented in Figure 7 in terms of the dimensionless torque on the surface of inner cylinder, G, as a function of the Reynolds number, Re. Similar to the case of the TC, the agreement between the experiments and the simulations is satisfactory. This confirms the validity of the adopted procedure in our CFD simulations. Therefore, the same procedure is used in the following also for the other geometries.

To investigate the effect of the deformation of the inner cylinder on the flow pattern in the gap of the LTC unit we keep the minimum gap width, d_{min}, constant, equal to 8 mm, and vary the maximum gap width, d_{max}. The obtained radial velocity patterns on the unwrapped circumferential surface in the middle of the smallest gap ($R = 62$ mm) are shown in Figure 8a–d, respectively for (a) $d_{max} = 10$ mm, (b) $d_{max} = 12$ mm, (c) $d_{max} = 16$ mm, and (d) $d_{max} = 22$ mm. Note that in all cases the flow is turbulent, and the rotation speed has been adjusted so to have the volume averaged shear rate equal to $\langle\gamma\rangle = 685\ s^{-1}$. By comparing Figure 8a–d with Figure 2b, it is seen that changing the cross section profile of the inner cylinder has a substantial effect on the flow patterns in the LTC unit. When the difference between d_{max} and d_{min} is small, as in the case of Figure 8a, only small deformation of the toroidal vortexes can be observed. Further increase in the difference between d_{max} and d_{min} leads to the flow patterns at each fixed point with respect to the nonrotational outer cylinder varying periodically in the circumferential direction. Obviously, such periodic variations will depend on the shape of the inner cylinder, and for the particular case of the triangular cross section, the period is 1/3 of the time for one rotation of the inner cylinder. The periodic flow variations have also been observed experimentally by Snyder[31] for a TC unit with the inner cylinder of a square cross section.

In Figure 9a–d are presented the corresponding velocity vectors in the vertical surfaces located in the smallest and largest gap of the LTC. The size of the arrow indicates the absolute velocity magnitude and the color represents the magnitude of the radial velocity component. As can be seen, increasing the maximum gap width d_{max} increases also the size of the vortexes and consequently decreases their number. The shape of the vortexes in the maximum gap in Figure 9a–d is approximately circular, while it is progressively elongated in the minimum gap as d_{max} increases. This means that the maximum wavelength, λ_{max}, defined as the ratio of the vertical extent of two toroidal vortexes, l, to the maximum gap, d_{max}, stays approximately constant, but the minimum wavelength, λ_{min}, defined as the ratio of the vertical extent of two toroidal vortexes, l, to the minimum gap, d_{min}, increases as the difference between d_{min} and d_{max} increases. In the case of a TC unit with eccentrically located inner cylinder, Koschmieder[25] observed experimentally that the λ_{max} value decreases and the λ_{min} value increases monotonically as the difference between d_{min} and d_{max} increases. This clearly indicates the different flow features between the TC with eccentric cylinders and the present LTC. Moreover, as observed by various authors[25–29] when the inner cylinder eccentricity is large the reverse flow may occur in the region of maximum gap. Such reverse flow instead does not appear in the LTC units investigated in this work.

Figure 10 compares the distributions of the normalized shear rate for the LTC units with triangle cross-section of the inner cylinder at four different values of $d_{max} = 12$, 16, 22, and 31 mm, together with those obtained for the TC and the ST units. Note that in the case of the largest gap width $d_{max} = 31$ mm, the cross-section profile of the triangle inner cylinder cannot be constructed by connecting the three circles along their mutual tangential lines. Instead, they are connected with circles of radius $R_c = 30$ mm, as shown in Figure 11. The position of the circles with respect to the center of the LTC are given by $e_1 = 32$ mm and $e_2 = 69.215$ mm. It is seen that as the maximum gap width d_{max} increases, the shear rate distribution becomes narrower, and for $d_{max} \geq 16$ mm the distribution is substantially narrower than those of the ST and the TC units covering approximately one order of magnitude. Moreover, with respect to the ST, the normalized shear rate distributions of the LTC units exhibit much shorter tails, particularly in the region of large shear rates. On the

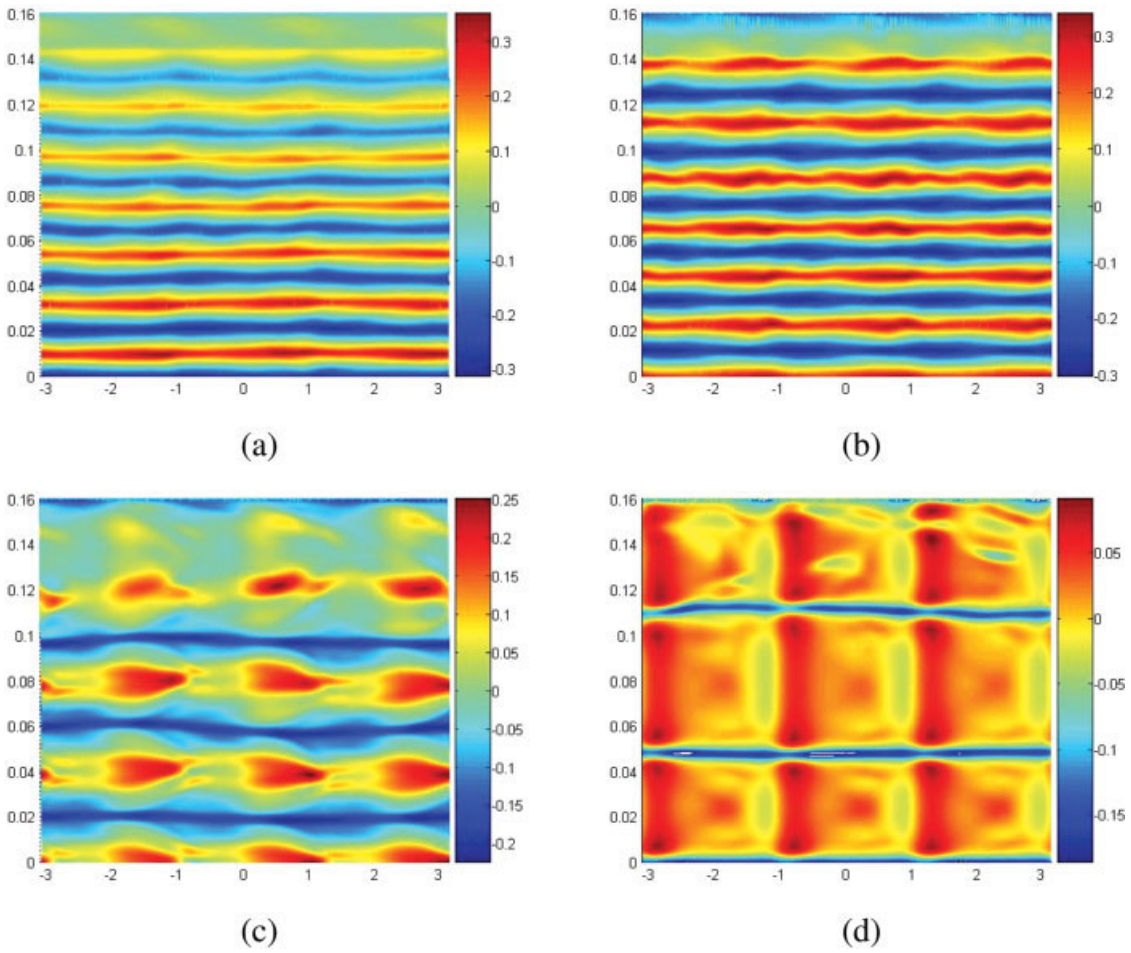

Figure 8. Radial velocity pattern on the unwrapped circumferential surface in the middle of the smallest gap for the LTC unit with triangular profile of the inner cylinder cross section: (a) d_{max} = 10 mm; (b) d_{max} = 12 mm; (c) d_{max} = 16 mm; (d) d_{max} = 22 mm.

[Color figure can be viewed in the online issue, which is available at www.interscience.wiley.com.]

other hand, with respect to the TC unit, the main difference is in the region of small shear rates, which has been clearly reduced in the case of the LTC units. This is due to the temporal-periodic variations of the flow pattern in the LTC units, which significantly deform the Taylor vortexes and eliminates the low velocity gradient (low shear rate) region located in the vortex core of the TC units.

However, further increasing the d_{max} value, such as in the case of $d_{max} = 31$ mm in Figure 10, leads to broadening the normalized shear rate distribution. This arises because at $d_{max} = 31$ mm, a different construction approach has been used for the inner cylinder, as given in Figure 11. This results in the form of the inner cylinder very similar to an impeller used in a ST, broadening the shear rate distribution. Therefore, in the design of the LTC units, to obtain a narrow shear rate distribution, we should keep the ratio between d_{max} and d_{min}, in a certain range, and based on our numerical simulations the recommended value is between two and three.

As a further check of the reliability of the simulation results reported earlier, the simulation of the LTC unit with $d_{max} = 16$ mm has been performed applying three different turbulent models: standard k-ε (SKE), renormalized group k-ε (RNG), and Reynolds stress model.[49] The computed normalized shear rate distributions are shown in Figure 12. It is seen that, although some slight differences in the normalized shear rate distributions appear, they are certainly insufficient to affect the conclusion drawn in the context of Figure 10 about the comparisons with the TC and ST units.

Another important parameter in industrial applications is the power input (power per unit volume) to the unit. For the above LTC units with the triangular inner cylinder cross-section, the power input (P/V), has been computed as a function of the gap width difference, δ ($=d_{max} - d_{min}$), for a fixed value of the volume-averaged shear rate, $\langle\gamma\rangle$ equal to 685 s^{-1}. The power, P, is estimated based on the computed total torque value on the surface of the inner cylinder:

$$P = \Omega\tau \tag{3}$$

In Figure 13 is shown the ratio of the power inputs of the LTC unit to that of the TC units, $R_{P/V}$, as a function of δ. It appears that the TC unit ($\delta = 0$) leads to the largest power input, while the power input of the LTC unit decreases as the

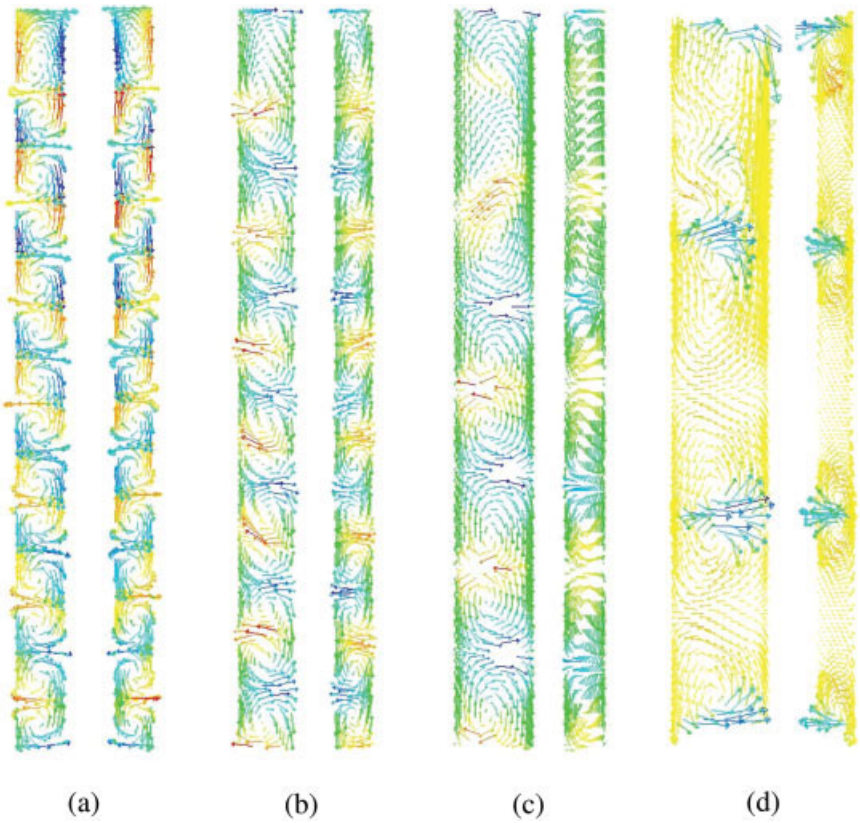

Figure 9. Flow fields in the maximum and minimum gaps of the LTC for various values of the maximum gap width corresponding to the flow patterns presented in Figure 8, (a) d_{max} = 10 mm, (b) d_{max} = 12 mm, (c) d_{max} = 16 mm and (d) d_{max} = 22 mm, where the color indicates the radial velocity.

[Color figure can be viewed in the online issue, which is available at www.interscience.wiley.com.]

δ value increases. This arises mostly because at a fixed $\langle\gamma\rangle$ value, the surface-to-volume ratio is the largest for the TC and then decreases progressively with increasing the maximum gap width of the LTC unit. The results in Figure 13 show that in the region of $\delta \in (0, 8\text{ mm})$, the power input of the LTC unit decreases sharply as δ increases, while a further increase in δ does not lead to significant changes in the power input. This indicates that the energy efficiency for mixing is larger in the LTC than in the TC unit, thus leading to better mass and heat transport characteristics. It is worth mentioning in this context that the power input of a ST, for the same $\langle\gamma\rangle$ value, is smaller than both TC and LTC units.

Role of the shape of the inner cylinder cross section

We now investigate the effect of the shape of the inner cylinder cross section, while keeping constant the gap width difference δ of the LTC unit. In Figure 14 are shown the distributions of the normalized shear rate computed using three types of the inner cylinder cross-sections: elliptical, triangular, and square, with fixed values of $d_{max} = 16$ mm, $d_{min} = 8$ mm, and $\langle\gamma\rangle = 685\ s^{-1}$. For a comparison, the normalized shear rate distributions for the corresponding TC and ST units are also shown. It is seen that the shear rate distributions of the three cases are rather similar, with slightly larger tails in the case of the elliptical profile, but all of them are substantially narrower than those of the TC and the ST units.

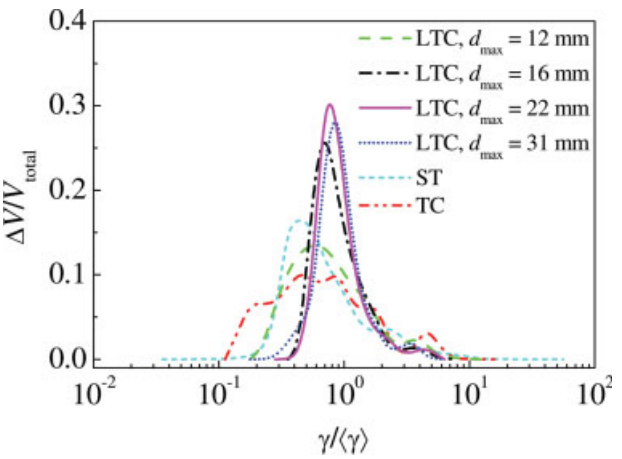

Figure 10. Distributions of the normalized shear rate, $\gamma/\langle\gamma\rangle$, in LTC units with triangular profile of the inner cylinder cross-section for various d_{max} values compared with those of the TC and ST units. R_o = 70 mm; d_{min} = 8 mm, = 685 s^{-1}.

[Color figure can be viewed in the online issue, which is available at www.interscience.wiley.com.].

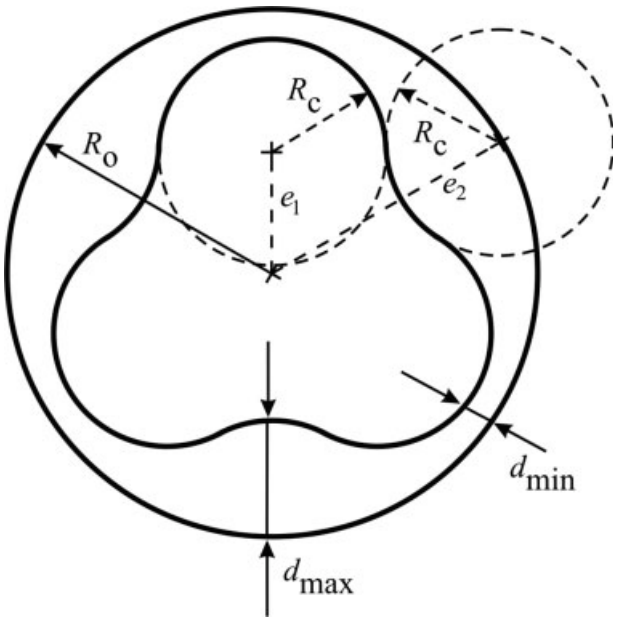

Figure 11. Schematic of the cross section of the inner cylinder perpendicular to the rotation axis of a lobed TC unit in the case of a triangle-type profile with d_{max} = 31 mm.

Of course, the situation would be different for different diameters of the inner and outer cylinders with the same gap width. However, in general as the diameter of the unit increases, a lobed inner cylinder cross-section with more lobes should be used in order to keep a narrow shear rate distribution for a given $\langle\gamma\rangle$ value.

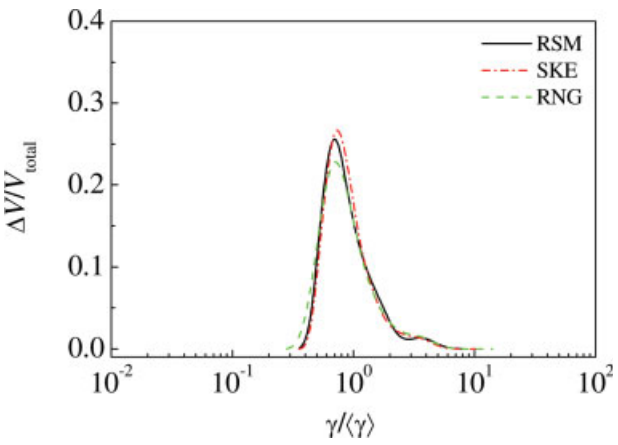

Figure 12. Distributions of the normalized shear rate calculated with three turbulence models for the LTC unit with triangular cross-section of the inner cylinder; R_o = 70 mm; d_{min} = 8 mm; d_{max} = 16 mm.

[Color figure can be viewed in the online issue, which is available at www.interscience.wiley.com.]

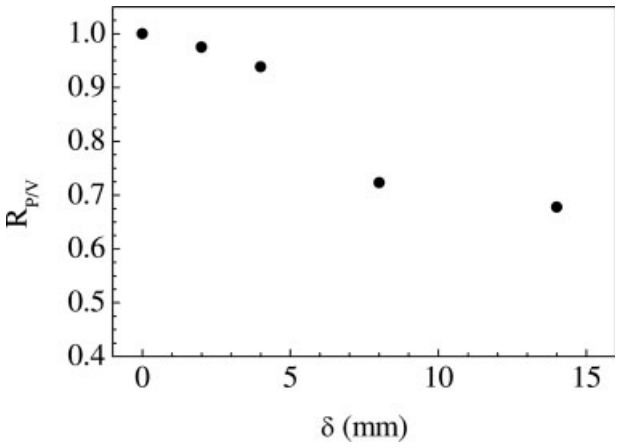

Figure 13. Ratio of the power input of the LTC to that of the TC unit, $R_{P/V}$, as a function of the difference between maximum and minimum gap widths, $\delta = d_{max} - d_{min}$, at a fixed value of $\langle\gamma\rangle$ = 685 s^{-1}.

Triangular inner cylinder cross-section; R_o = 70 mm; d_{min} = 8 mm.

Concluding Remarks

In this work a new type of mixing units based on a modification of the classical Taylor-Couette (TC) has been proposed. The circular cross-section of the inner cylinder of the TC unit has been replaced by a lobed cross-section whose detailed shape can be designed according to specific needs. This leads to a nonconstant gap width between inner and outer cylinders, and we refer to it as to the LTC unit. The main purpose of this modification is to deform and reduce the Taylor vortexes, characteristics of the TC unit, so as to obtain a narrower distribution of the shear rate. The feasibility of the proposed LTC unit has been investigated through

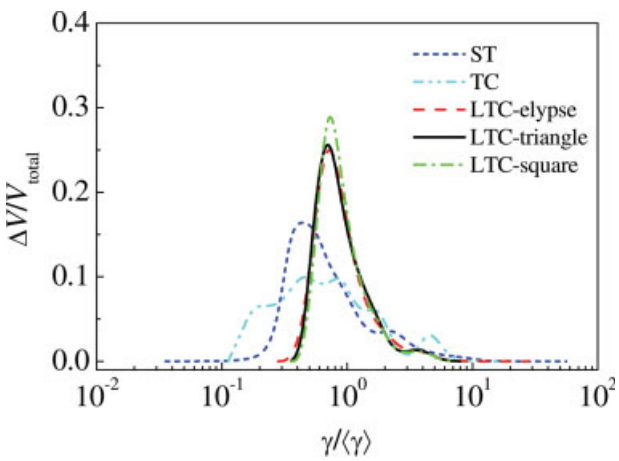

Figure 14. Distributions of the normalized shear rate calculated for the LTC units using elliptical, triangular and square inner cylinder cross-sections compared to those corresponding to the classical TC and the ST units: R_o = 70 mm; d_{min} = 8 mm; d_{max} = 16 mm.

[Color figure can be viewed in the online issue, which is available at www.interscience.wiley.com.]

numerical simulations using the commercial CFD package, Fluent v6.2.

It is found that for a fixed value of the volume-average shear rate $\langle\gamma\rangle$, the distribution of the normalized shear rate $\gamma/\langle\gamma\rangle$ in a generic LTC unit is substantially narrower than that in a TC unit or in a standard ST. The involved ranges of the $\gamma/\langle\gamma\rangle$ values can differ by orders of magnitude in the different units. The shape of the distributions in the LTC units is typically much more symmetric, with the peak position located very close to the average value $\langle\gamma\rangle$.

With respect to applications in mixing processes the LTC units offer some clear advantages. In the first place, the long tails in the region of high shear rates characteristic of the ST units are removed. This avoids the stirred material to undergo regions of very high shear rates, which can often alter the material properties or cause undesired breakage/aggregation events. In the second place, the regions with very low values of the shear rate present in the classical TC units have been removed in the LTC units. This is due to the fact that the flow pattern is temporal-periodic in each point of a LTC unit, and this eliminates the low velocity gradient (low shear rate) region located in the vortex core of the TC unit. This leads to improved efficiency of the interphase transport processes for multiphase systems.

The narrowest $\gamma/\langle\gamma\rangle$ distributions of the LTC units are obtained when the ratio of the largest to the smallest gap widths, d_{max}/d_{min}, is in the range from 2 to 3. Three polygonal (elliptical, triangular, and square) cross-sections of the inner cylinder have been investigated through CFD simulations. The triangular and square cross-sections lead to slightly narrower shear rate distributions, but in all cases the distributions exhibited by the LTC units are narrower than those of the TC and the ST units.

Acknowledgments

Financial support from the Swiss National Science Foundation (NSF, Grant No. 200020-101714) is gratefully acknowledged. Authors would like to acknowledge Markus Küpfer for his effort in constructing the LTC and the TC units.

Notation

d = gap width of the TC unit, m
d_{man} = maximum gap width of the LTC unit, m
d_{min} = minimum gap width of the LTC unit, m
D = impeller diameter, m
G = dimensionless torque, defined by Eq. 1
k = turbulent kinetic energy, m^2/s^2
L = length of the TC or LTC unit, m
N = rotation speed of the impeller, rpm
P = power consumed by the fluid motion, defined by Eq. 3, W
Q_r = liquid flow rate through the surface around the impeller
r = distance from the center of the stirred vessel, m
r^+ = dimensionless distance from the center of the stirred vessel
Re = Reynolds number of the TC unit, defined by Eq. 1
R = stirred vessel radius, m
R_i = radius of the inner cylinder of the TC unit, m
R_o = radius of the outer cylinder of the TC unit, m
$R_{P/V}$ = ratio of the power input between the LTC and TC units
U_{ax} = mean axial velocity component, m/s
U_r = mean radial velocity component, m/s
U_{tan} = mean tangential velocity component, m/s
V = volume of the fluid in the unit, m^3
V_{tip} = tip velocity of the impeller blade, m/s
W = height of the impeller blade, m
y = distance from the wall, m
y^+ = value of the wall units
z = axial distance from centre of the blade, m

Greek letters

γ = shear rate, s^{-1}
$\langle\gamma\rangle$ = volume-averaged shear rate, s^{-1}
$\delta = d_{max} - d_{min}$, m
ε = turbulent energy dissipation rate, m^2/s^3
$\eta = R_i/R_o$
ν = kinematic viscosity of the fluid, m^2/s
ρ = density of the fluid, kg/m^3
τ = torque on the rotating shaft, Nm
Ω = angular velocity, rad/s

Literature Cited

1. Kataoka K, Ohmura N, Kouzu M, Simamura Y, Okubo M. Emulsion polymerization of styrene in a continuous taylor vortex flow reactor. *Chem Eng Sci*. 1995;50:1409–1416.
2. Wei X, Takahashi H, Sato S, Nomura M. Continuous emulsion polymerization of styrene in a single Couette-Taylor vortex flow reactor. *J Appl Polym Sci*. 2001;80:1931–1942.
3. Hallström B, Lopez-Leiva M. Description of a rotating ultrafiltration module. *Desalination* 1978;24:273–279.
4. Kroner KH, Nissinen V, Ziegler H. Improved dynamic filtration of microbial suspensions. *Biotechnology* 1987;5:921.
5. Kroner KH, Nissinen V. Dynamic filtration of microbial suspensions using an axially rotating filter. *J Membr Sci*. 1988;36:85–100.
6. Winzeler HB, Belfort G. Enhanced performance for pressure driven membrane processes: The argument for fluid instabilities. *J Membr Sci*. 1993;80:35–47.
7. Margaritis A, Wilke CR. The rotorfermentor. I. Description of the apparatus, power requirements, and mass transfer characteristics. *Biotechnol Bioeng*. 1978;20:709–726.
8. Margaritis A, Wilke CR. The rotorfermentor. II. Application to ethanol fermentation. *Biotechnol Bioeng*. 1978;20:727–753.
9. Haut B, Ben Amor H, Coulon L, Jaquet A, Halloin V. Hydrodynamics and mass transfer in a Couette-Taylor bioreactor for the culture of animal cells. *Chem Eng Sci*. 2003;58:777–784.
10. Ameer GA, Barabino G, Sasisekharan R, Harmon W, Cooney CL, Langer R. Ex-vivo evaluation of a Taylor-Couette flow, immobilized heparinase I device for clinical application. *Proc Natl Acad Sci USA*. 1999;96:2350–2355.
11. Ameer GA, Grovender EA, Obradovic B, Cooney CL, Langer R. RTD analysis of a novel Taylor-Couette flow device for blood detoxification. *AIChE J*. 1999;45:633–638.
12. Ameer GA, Harmon W, Sasisekharan R, Langer R. Investigation of a whole blood fluidized bed Taylor-Couette flow device for enzymatic heparin neutralization. *Biotechnol Bioeng*. 1999;62:602–608.
13. Ameer GA, Raghavan S, Sasisekharan R, Harmon W, Cooney CL, Langer R. Regional heparinization via simultaneous separation and reaction in a novel Taylor-Couette flow device. *Biotechnol Bioeng*. 1999;63:618–624.
14. Barresi AA, Marchisio DL, Baldi G. On the role of micro- and mesomixing in a continuous Couette-type precipitator. *Chem Eng Sci*. 1999;54:2339–2349.
15. Sczechowski JG, Koval CA, Noble RD. A taylor vortex reactor for heterogeneous photocatalysis. *Chem Eng Sci*. 1995;50:3163–3173.
16. Haim D, Pismen LM. Performance of a photochemical reactor in the regime of Taylor-Gortler vortical flow. *Chem Eng Sci*. 1994;49:1119–1129.
17. Vel Leitner NK, Le Bras E, Foucault E, Bousgarbies J-M. A new photochemical reactor design for the treatment of absorbing solutions. *Water Sci Technol*. 1997;35:215–222.
18. Sengupta TK, Kabir MF, Ray AK. A Taylor vortex photocatalytic reactor for water purification. *Ind Eng Chem Res*. 2001;40:5268–5281.
19. Kabir MF, Ray AK. Performance enhancement of a chemical reactor utilizing flow instability. *J Chem Technol Biotechnol*. 2003;78:314–320.
20. Dutta PK, Ray AK. Experimental investigation of Taylor vortex photocatalytic reactor for water purification. *Chem Eng Sci*. 2004;59:5249–5259.

21. Baier G, Graham MD, Lightfoot EN. Mass transport in a novel two-fluid Taylor Vortex extractor. *AIChE J*. 2000;46:2395–2407.
22. Desmet G, Verelst H, Baron GV. Local and global dispersion effects in Couette-Taylor flow-II. Quantitative measurements and discussion of the reactor performance. *Chem Eng Sci*. 1996;51:1299–1309.
23. Resende MM, Tardioli PW, Fernandez VM, Ferreira ALO, Giordano RLC, Giordano RC. Distribution of suspended particles in a Taylor-Poiseuille vortex flow reactor. *Chem Eng Sci*. 2001;56:755–761.
24. Drozdov SM. A numerical investigation of a modified Couette-Taylor apparatus with application to industrial mixing. *Theor Comput Fluid Dyn*. 2002;16:17–28.
25. Koschmieder EL. Taylor vortices between eccentric cylinders. *Phys Fluids*. 1976;19:1–4.
26. Szeri AZ, Al-Sharif A. Flow between finite, steadily rotating eccentric cylinders. *Theor Comput Fluid Dyn*. 1995;7:1–28.
27. Dris I, Shaqfeh ESG. Flow of a viscoelastic fluid between eccentric cylinders: impact on flow stability. *J Non-Newtonian Fluid Mech*. 1998;80:59–87.
28. Versteegen PL, Jankowski DF. Experiments on the stability of viscous flow between eccentric rotating cylinders. *Phys Fluids*. 1969;12:1138–1143.
29. Tennakoon SGK, Andereck CD. Time-dependent patterns in counter-rotating eccentric cylinders. *Phys Rev Lett*. 1993;71:3111–3114.
30. Lopez JM, Marques F. Modulated Taylor-Couette flow: Onset of spiral modes. *Theor Comput Fluid Dyn*. 2002;16:59–69.
31. Snyder HA. Experiments on rotating flows between noncircular cylinders. *Phys Fluids*. 1968;11:1606–1611.
32. Mullin T, Lorenzen A. Bifurcation phenomena in flows between a rotating circular cylinder and a stationary square outer cylinder. *J Fluid Mech*. 1985;157:289–303.
33. Wu H, Soos M, Morbidelli M. Rotating stirring device with substantially narrow distribution of energy dissipation rate. EU Patent 03019330.4, 2003.
34. Camp TR, Stein PC. Velocity gradients and internal work in fluid motion. *J Boston Soc Civil Eng*. 1943;30:219–237.
35. Wu H, Patterson GK. Laser-Doppler measurements of turbulent-flow parameters in a stirred mixer. *Chem Eng Sci*. 1989;44:2207–2221.
36. Yoon HS, Sharp KV, Hill DF, Adrian RJ, Balachandar S, Ha MY, Kar K. Integrated experimental and computational approach to simulation of flow in a stirred tank. *Chem Eng Sci*. 2001;56:6635–6649.
37. Fan JH, Wang YD, Rao Q, Fei WY. A study on intermittency phenomena in the impeller stream via digital particle image velocimetry (DPIV). *Chem Eng J*. 2004;102:25–33.
38. Escudie R, Line A. Experimental analysis of hydrodynamics in a radially agitated tank. *AIChE J*. 2003;49:585–603.
39. Bugay S, Escudie R, Line A. Experimental analysis of hydrodynamics in axially agitated tank. *AIChE J*. 2002;48:463–475.
40. Sheng J, Meng H, Fox RO. Validation of CFD simulations of a stirred tank using particle image velocimetry data. *Can J Chem Eng*. 1998;76:611–625.
41. Zhu X, Vigil RD. Banded liquid-liquid Taylor-Couette-Poiseuille flow. *AIChE J*. 2001;47:1932–1940.
42. Campolo M, Sbrizzai F, Soldati A. Time-dependent flow structures and Lagrangian mixing in Rushton-impeller baffled-tank reactor. *Chem Eng Commun*. 2003;58:1615–1629.
43. Mavros P, Mann R, Vlaev SD, Bertrand J. Experimental visualization and CFD simulation of flow patterns induced by a novel energy-saving dual-configuration impeller in stirred vessels. *Chem Eng Res Des*. 2001;79:857–866.
44. Marchisio DL, Barresi AA, Fox RO. Simulation of turbulent precipitation in a semi-batch Taylor-Couette reactor using CFD. *AIChE J*. 2001;47:664–676.
45. Koschmieder EL. Turbulent Taylor vortex flow. *J Fluid Mech*. 1979;93:515–527.
46. Lathrop DP, Fineberg J, Swinney HL. Transition to shear-driven turbulence in Couette-Taylor flow. *Phys Rev A*. 1992;46:6390–6405.
47. Wendt F. Turbulente Strömungen zwischen zwei rotierenden konaxialen Zylindern. *Ing Arch*. 1933;4:577.
48. Campero RJ, Vigil RD. Spatiotemporal patterns in liquid-liquid Taylor-Couette-Poiseuille flow. *Phys Rev Lett*. 1997;79:3897–3900.
49. Fluent. Fluent 6.2 User's Guide. Lebanon, NH:Fluent, 2005.

Appendix: Validation of the CFD Simulations of the Stirred Tank by Wu and Patterson[35]

The stirred tank (ST) considered in our simulations is the same one used by Wu and Patterson[35] for the LDA measurements. It has a standard geometry with diameter of 270 mm and is equipped with a Rushton turbine. The initial computational grid contains approximately 170,000 cells, and stand-

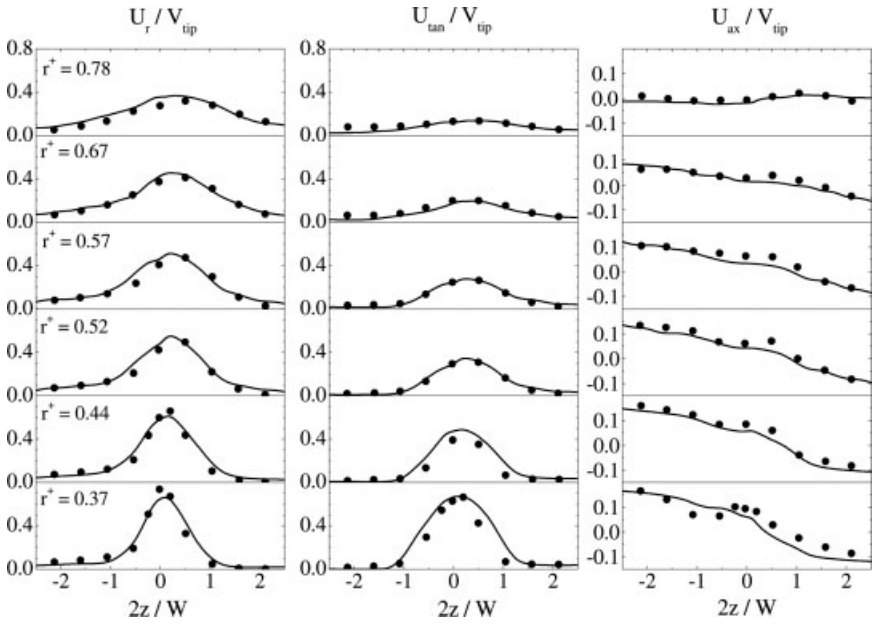

Figure A1. Profiles of the mean velocity components in radial (U_r), tangential (U_{tan}), and axial (U_{ax}) directions, normalized by the turbine tip velocity (V_{tip}), in the stirred tank used by Wu and Patterson.[35] (●) LDA data by Wu and Patterson,[35] (—) CFD simulations.

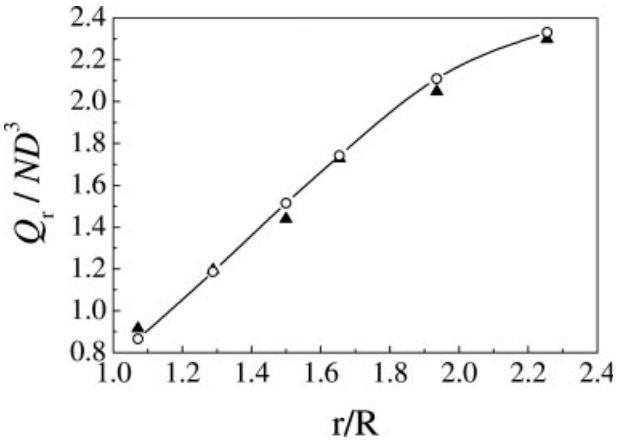

Figure A2. Comparison between the profiles of the radial discharge flow number measured (▲) by Wu and Patterson,[35] and simulated (–○–) by CFD.

ard k-ε model with standard wall function is used.[42] After the transient simulation reaches pseudo steady-state, the grid is adapted based on predefined threshold values for the maximum velocity gradient. Since the shear rate distribution is sensitive on the distance of the first elements from the solid wall also in the case of ST the values of y^+ was kept approximately the same as in the TC and LTC simulations. The final grid contains slightly more than 700,000 computational cells.

Figure A1 compares the computed profiles of the radial, tangential and axial velocity components normalized by the blade tip velocity at the rotation speed of 200 rpm with the corresponding LDA measurements.[35] It is seen that the agreement between simulation results and LDA measured data is satisfactory. Wu and Patterson[35] reported also the radial variations of the discharging flow, Q_r. In the CFD simulations, we have calculated Q_r based on the integral mass flow rate through cylindrical surfaces around the impeller. The calculated values of the discharging flow number, (where N is the rotation speed and D is the diameter of the turbine), are compared with the experimental data in Fig. A2. Good agreement is obtained both near the impeller and in the wall region. This indicates that the development of the discharging stream has been well simulated in the different regions of the ST.

Manuscript received Aug. 19, 2005, and revision received Feb. 5, 2007.